Bifurcations in a Two-Mode Semiconductor Laser with Optical Injection

Nicholas Blackbeard, Simon Osborne, Stephen O'Brien, Andreas Amann

Bifurcations in a Two-Mode Semiconductor Laser with Optical Injection

Nicholas Blackbeard[†], Simon Osborne[†], Stephen O'Brien[†] and Andreas Amann[†‡].

†Tyndall National Institute, University College Cork, Ireland
‡School of Mathematical Sciences, University College Cork, Ireland
Email: nicholas.blackbeard@tyndall.ie

Abstract—We explore an unusual bursting mechanism in a two-mode semiconductor laser with single-mode optical injection. By changing the injection strength and frequency detuning (between the injected mode and the injected light) we find a striking transition from purely single-mode intensity oscillations to sudden bursting in the intensity of the second mode. This phenomenon is organised by a pair of codimension-two bifurcations which are formed by interactions between saddle-node and pitchfork (of limit cycles) bifurcations.

1. Introduction

Bursting is a striking feature of a wide range of physical and biological systems. Well known examples include neuroscience [1], the Taylor–Couette flow [2, 3], and turbulence in boundary layers [4, 5]. Furthermore, if invariant manifolds or symmetries are present in the underlying systems one can find unusual mechanisms that lead to bursting, e.g. bubbling and riddled-basins [6, 7]. A better understanding of the mechanisms responsible for bursting in systems with invariant manifolds would be of wider interest.

In this paper we study an experimentally accessible and technologically relevant example of a system with an invariant manifold that exhibits bursting, namely an optically injected two-mode semiconductor laser.

2. Experimental Setup

The device we use is a multi-quantum well InGaAlP/InP Fabry-Perot (FP) laser of length 350μm. Mode selection is achieved by perturbing the FP spectrum using slotted regions etched into the ridge waveguide. Further details of the design of these lasers and their free running characteristics can be found in Ref. [8]. Figure 1 shows the optical spectrum of the two-mode laser. The large frequency spacing (~480 GHz) results in a weak coupling between the two modes and therefore stable and simultaneous lasing.

For our experiment, the two-mode laser is in a temperature controlled environment and is used in the master-slave configuration, as shown in Fig. 1. Light from the master laser, a tunable laser with less than 100 kHz linewidth, is injected into the long wavelength mode of the slave, two-mode laser. We use optical isolators to eliminate unwanted optical feedback, in-line fibre bandpass filters to monitor
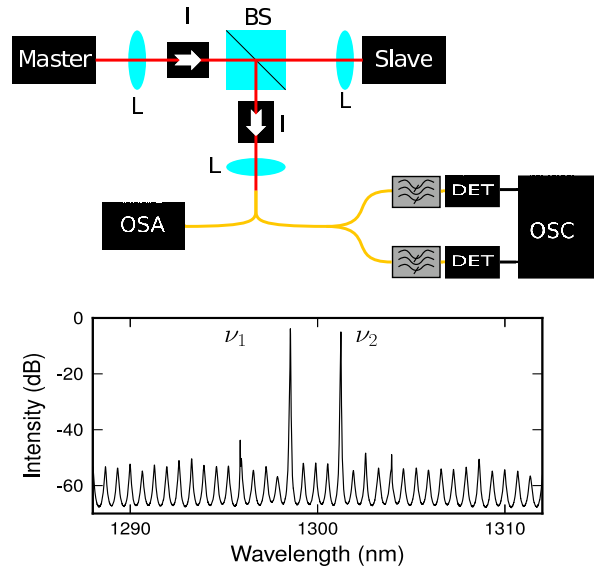

Figure 1: Top: experimental setup of a two-mode laser (slave) with single-mode injection (master). Bottom: the spectrum of the free-running two-mode laser.

each of the modes, and the bandwidth of our system is 8 GHz.

3. Laser Rate Equations

A simple four-dimensional set of ODEs has been shown to accurately capture a number of experimentally observed dynamical phenomena for the setup shown in Fig. 1. The time-dependent variables in this model are: the magnitude of the uninjected mode, $|E_1(t)|$, the complex field of the injected mode, $E_2(t)$, and the excess carrier density, $N(t)$. In dimensionless form it is given by [9]

$$
\begin{aligned}
\frac{d|E_1|}{dt} &= \frac{1}{2}((2N+1)g_1 - 1)|E_1|, \\
\frac{dE_2}{dt} &= \left[\frac{1}{2}((2N+1)g_2 - 1)(1+i\alpha) - i\Delta\omega\right]E_2 + K, \\
T\frac{dN}{dt} &= P - N - (1+2N)\sum_{m=1}^{2} g_m|E_m|^2.
\end{aligned}
\tag{1}
$$

The bifurcation parameters are the normalised strength of the injected light, K, and the normalised frequency detuning between the injected mode and the injected light, $\Delta\omega$.

Further parameters are the coupling, α, between the magnitude and phase of E_2; the product of carrier lifetime and the cavity decay rate, T; and the normalised pump current, P. The two modes are coupled through $N(t)$ via the nonlinear modal gain

$$g_1 = \left[1 + \epsilon \left(\beta_{11}|E_1|^2 + \beta_{12}|E_2|^2 \right) \right]^{-1} ,$$

$$g_2 = \left[1 + \epsilon \left(\beta_{21}|E_1|^2 + \beta_{22}|E_2|^2 \right) \right]^{-1} ,$$

where $\epsilon\beta_{mm}$ is the self saturation of a mode, and $\epsilon\beta_{mn}$ ($m \neq n$) is the cross saturation between modes. For this paper we fix $\epsilon = 0.1$, $\beta_{11} = \beta_{22} = 1$, $\beta_{12} = \beta_{21} = \frac{2}{3}$, $\alpha = 2.6$, $T^{-1} = 0.00125$, and $P = 0.5$ (twice threshold).

The phase space of system (1) features a three-dimensional sub-manifold,

$$\mathcal{M} = \{ \ (|E_1|, \mathrm{Re}(E_2), \mathrm{Im}(E_2), N) \ \in \mathbb{R}^4 \ : \ |E_1| = 0 \ \},$$

which is invariant under the time evolution of (1). We refer to $\mathcal{M}$ as the *single-mode manifold* since the dynamics on $\mathcal{M}$ reduce to that of the well-studied single-mode injection problem [10, 11]. To facilitate our discussion we term attractors of system (1) *single-mode attractors* if they are contained in $\mathcal{M}$, and *two-mode attractors* if not. A single-mode attractor corresponds to only the injected mode being 'on', whereas a two-mode attractor correspond to both modes being 'on'. We also note that system (1) has a formal $\mathbb{Z}_2$ symmetry due to the transformation $|E_1| \to -|E_1|$. Physically, only positive field magnitudes are relevant.

4. Local Bifurcation Analysis

The global bifurcation structure of system (1) has been reported in Ref. [9]. Here we focus on a region of the $(K, \Delta\omega)$ parameter plane (Fig. 2) with interesting transitions from a single-mode limit cycle (grey shading) to a two-mode attractor (no shading).

In Fig. 2 the boundary of the grey region contains two saddle-node-pitchfork of limit cycle (SPL) bifurcation points. These two points are formed by tangencies between a curve of saddle-node of limit cycle (SL) bifurcations and a curve of pitchfork of limit cycle (PL) bifurcations. Connecting the two SPL points is a curve of supercritical torus (T) bifurcations. A two-mode torus is created when this curve is crossed by increasing $\Delta\omega$.

The SPL points divide the grey region's boundary into three segments. From left to right in Fig. 2, the first and last segments correspond to curves of supercritical PL bifurcations. Crossing either of these segments by decreasing $\Delta\omega$ results in two stable two-mode limit cycles bifurcating out of the single-mode manifold $\mathcal{M}$. The magnitude of the uninjected mode is negative for one of these limit cycles and so we discuss it no further. The middle segment of the grey region's boundary corresponds to a curve of SL bifurcations. Crossing this segment by decreasing $\Delta\omega$ destroys a stable single-mode limit cycle.
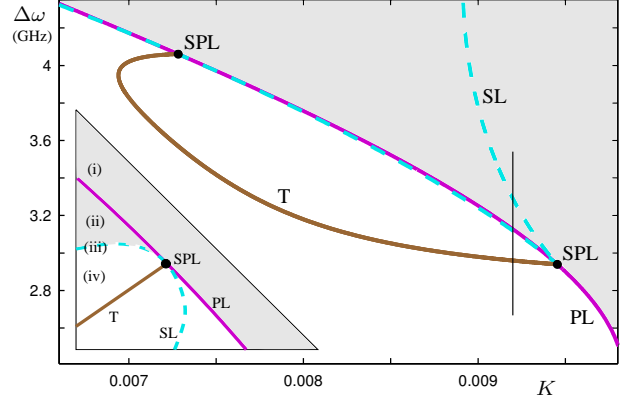

Figure 2: Two-parameter bifurcation diagram. Bifurcations of limit cycles are saddle-node (SL), pitchfork (PL), torus (T), and saddle-node-pitchfork (SPL). The grey shading is the stability region of a single-mode limit cycle. Inset: a sketch showing the arrangement of bifurcation curves close to the SPL point at high K.
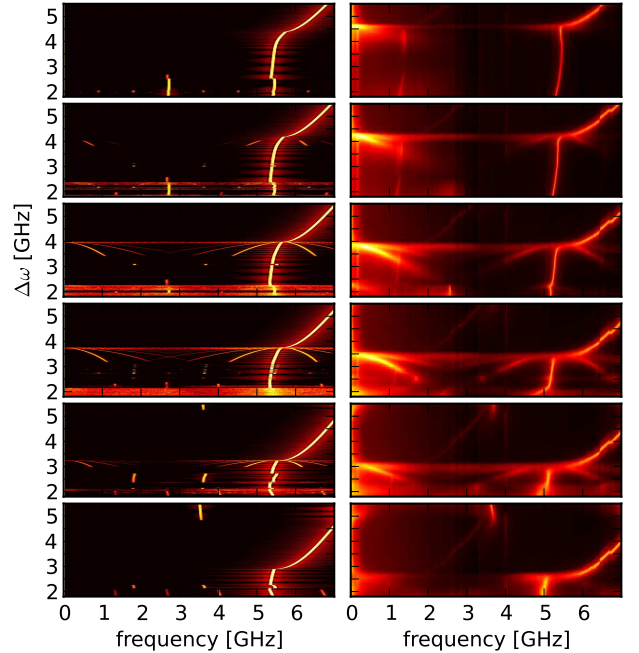

Figure 3: Power spectra of the injected mode as a function of the detuning $\Delta\omega$ obtained from numerics (left) and experiment (right). The strength of the injected light increases from $K = 0.006$ (top row) to $K = 0.0095$ (bottom row).
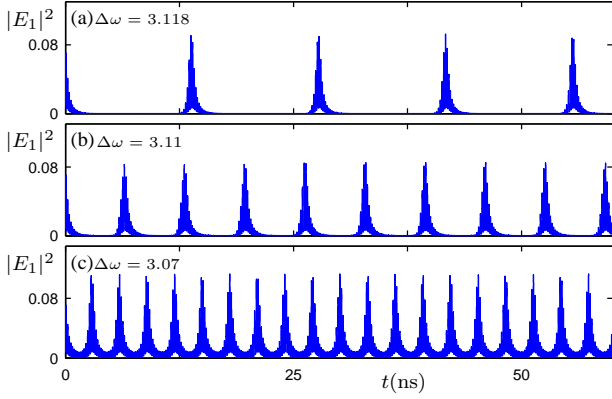
Figure 4: Time series of the uninjected mode for $K = 0.0092$ and different values of $\Delta\omega$ along the black line in Fig. 2. Decreasing $\Delta\omega$ causes the frequency of the bursts to increase.

To illustrate the transitions from a single-mode limit cycle to a two-mode attractor we present power spectra of the injected mode in Fig. 3. Each row corresponds to a different fixed value of the injection strength K, and the power spectra are shown as functions of the frequency detuning $\Delta\omega$. The agreement between the numerically calculated power spectra (left column of Fig. 3) and the experimentally measured power spectra (right column of Fig. 3) is excellent, and justifies a deeper analysis of the dynamics in system (1). Let us first consider row 1. For high $\Delta\omega$ the system has a dominant frequency which corresponds to beating between the injected light and the injected mode. Lowering $\Delta\omega$ causes the dominant frequency to decrease and then remain approximately constant at the relaxation oscillation. We also see this same structure in row 6 and identify it as being due to supercritical PL bifurcations on the boundary of the grey region in Fig. 2. The power spectra in rows 2–5 are qualitatively similar so we just describe row 4. Again, at high $\Delta\omega$ the system has a dominant frequency. However, when $\Delta\omega$ is decreased, a star-like structure develops. This star-like structure is a consequence of low frequency oscillations that are also visible in the power spectra. The star-like structure and low frequency oscillations in rows 2–5 are not fully explained by local SL bifurcations alone. We also need to consider global aspects of the dynamics in system (1).

5. Global Bifurcations Lead to Bursting

The low frequency oscillations detected in Fig. 3 are associated with bursting dynamics. Figure 4 contains time series of the uninjected-mode for parameter values below SL and along the black vertical line in Fig. 2. For frequency detunings $\Delta\omega$ close to the SL bifurcation curve there are large intervals of time where trajectories of system (1) stay close to the single-mode manifold $\mathcal{M}$, followed by
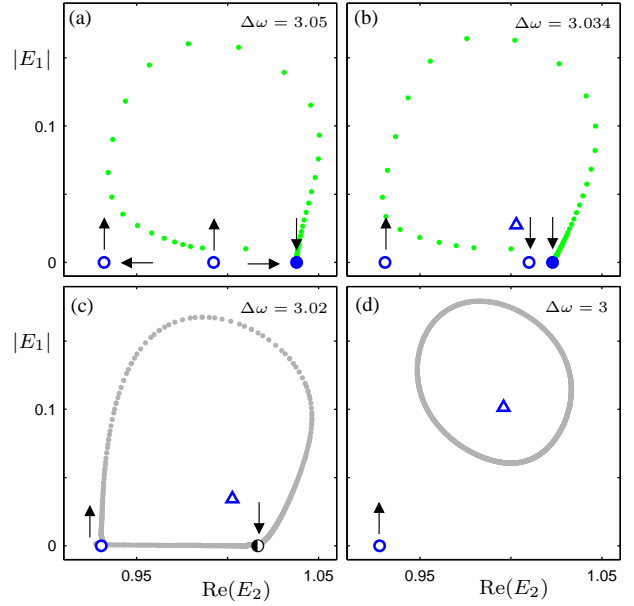

Figure 5: Two-dimensional projections from the Poincaré section defined by $Im(E_2) = 0$. (a)–(d) are representative of the dynamics in regions (i)–(iv) from Fig. 2. Fixed-points correspond to single-mode (circles), and two-mode (triangles) limit cycles. Their stability is indicated by shading: full=stable, open=unstable, and half-full=nonhyperbolic. $K = 0.00933$.

shorter time intervals where trajectories make excursions away from $\mathcal{M}$. These excursions show up as bursts in the uninjected mode (Fig. 4(a)). Moving away from the SL bifurcation curve (decreasing $\Delta\omega$) causes the frequency of the bursts to increase (Fig. 4(b)–(c)). This bursting behaviour is a consequence of a global bifurcation which we now describe with the aid of a Poincaré section.

Figure 5 contains two-dimensional projections from the Poincaré section defined by $Im(E_2) = 0$. In these projections the line $|E_1| = 0$ corresponds to the single-mode manifold $\mathcal{M}$, and fixed-points correspond to limit cycles of system (1). We start with parameter values from region (i) of Fig. 2. Here, system (1) has three single-mode limit cycles, one of which is stable (Fig. 5(a)). Decreasing $\Delta\omega$ through the PL bifurcation curve into region (ii) of Fig. 2 results in an unstable two-mode limit cycle bifurcating out of the single-mode manifold $\mathcal{M}$, and the middle single-mode limit cycle gaining transverse stability (Fig. 5(b)). Decreasing $\Delta\omega$ further leads to two simultaneous events. First, two single-mode limit cycles collide and form a non-hyperbolic limit cycle which is transversally stable. Second, a heteroclinic cycle is formed which connects the non-hyperbolic limit cycle to a transversally unstable limit cycle (Fig. 5(c)). This global bifurcation occurs along the SL bifurcation curve marked by (iii) in Fig. 2, close to the SPL bifurcation point. Decreasing $\Delta\omega$ further into region (iv) of Fig. 2 causes the nonhyperbolic limit cycle to disappear

and leads to the creation of stable torus (Fig. 5(d)).

The mechanism for bursting close to the right-most SPL point is thus as follows: for $(K, \Delta\omega)$ close to but below the curve marked by a (iii) in Fig. 2, trajectories spend along time travelling through a slow region of phase space close to the single-mode manifold $\mathcal{M}$. While trajectories are travelling through this region they are attracted toward $\mathcal{M}$. Once through the slow region they shadow the dynamics in $\mathcal{M}$ and are thus attracted to a transversally unstable single-mode limit cycle. The trajectories are then repelled away from $\mathcal{M}$ and then globally reinjected via the torus.

6. Summary

We studied, theoretically and experimentally, a two-mode semiconductor laser with single-mode injection. By changing the strength and frequency of the injected light we identified two contrasting transitions from single-mode oscillations to two-mode oscillations. On the one hand, a supercritical pitchfork of limit bifurcation leads to a gradual turning on of the uninjected mode. On the other hand, a saddle-node bifurcation of global type leads to sudden bursts in the magnitude of the uninjected mode.

References

[1] E. M. Izhikevich. Neural excitability, spiking and bursting. *Int. J. Bifurcat. Chaos*, 10(6):1171–1266, 2000.

[2] T. Mullin anf K. A. Cliffe. Unusual time-dependent phenomena in Taylor–Couette flow at moderately low Reynolds numbers. *Phys. Rev. Lett.*, 58(21):2212–2215, 1987.

[3] J. Abshagen, J. M. Lopez, F. Marques, and G. Pfister. Bursting dynamics due to a homoclinic cascade in Taylor–Couette flow. *J. Fluid Mech.*, 613:357–384, 2008.

[4] S. J. Kline, W. C. Reynolds, F. A. Schraub, and P. W. Runstadler. The structure of turbulent boundary layers. *J. Fluid Mech.*, 30(4):741–773, 1967.

[5] D. O. ReVelle. Chaos and bursting in the planetary boundary layer. *J. Appl. Meteorol.*, 32:1169–1180, 1993.

[6] P. Ashwin, J. Buescu, and I. Stewart. Bubbling of attractors and synchronisation of chaotic oscillators. *Phys. Lett. A*, 193:126–139, 1994.

[7] E. Ott. *Chaos in dynamical systems*. Cambridge University Press, New York, 2002.

[8] S. Osborne, S. O'Brian, K. Buckley, R. Fehse, A. Amann, J. Patchell, B. Kelly, D. E. Jones, J. O'Gorman, and E. P. O'Reilly. Design of single-mode and two-color Fabry-Perot lasers with patterned refractive index. *IEEE J. Sel. Topics Quantum Elecron.*, 13:1157–1163, 2007.

[9] S. Osborne, A. Amann, K. Buckley, G. Ryan, S. P. Hegarty, G. Huyet, and S. O'Brien. Antiphase dynamics in a multimode semiconductor laser with optical injection. *Phys. Rev. A*, 79:023834, 2009.

[10] S. Wieczorek, B. Krauskopf, T. B. Simpson, and D. Lenstra. The dynamical complexity of optically injected semiconductor lasers. *Phys. Rep.*, 416(1-2):1–128, 2005.

[11] B. Kelleher, C. Bonatto, G. Huyet, and S. P. Hegarty. Excitability in optically injected semiconductor lasers: Contrasting quantum-well- and quantum-dot-based devices. *Phys. Rev. E*, 83(026207), 2011.